Molecular Cell, Vol. 17, 181–191, January 21, 2005, Copyright ©2005 by Elsevier Inc. DOI 10.1016/j.molcel.2004.11.054

A Polybasic Motif Allows N-WASP to Act as a Sensor of PIP_2 Density

Venizelos Papayannopoulos,[1] Carl Co,[1] Kenneth E. Prehoda,[3] Scott Snapper,[2] Jack Taunton,[1] and Wendell A. Lim[1,*]
[1]Department of Cellular and Molecular Pharmacology and Program in Biological Sciences
University of California, San Francisco
San Francisco, California 94143
[2]Department of Medicine
Massachusetts General Hospital
Boston, Massachusetts 02114

Summary

Phosphatidylinositol 4,5-bisphosphate (PIP_2) activates the actin regulatory protein N-WASP by binding to a short polybasic region involved in N-WASP autoinhibition. Here, we show that unlike canonical lipid binding modules, such as PH domains, this polybasic motif binds PIP_2 in a multivalent, cooperative manner. As a result, PIP_2 activation of N-WASP-mediated actin polymerization in vitro and in extracts is ultrasensitive: above a certain threshold, N-WASP responds in a switch-like manner to a small increase in the density of PIP_2 (Hill coefficient $n_H = \sim 20$). We show that the sharpness of the PIP_2 activation threshold can be tuned by varying the length of the polybasic motif. This sharp activation threshold may help suppress N-WASP activation by quiescent PIP_2 levels yet leave it poised for activation upon subtle, signaling-induced perturbations in PIP_2 distribution.

Introduction

Phosphoinositides are employed as secondary signaling molecules in a diverse array of cellular pathways including those regulating cytoskeletal dynamics and vesicular trafficking (Cantley, 2002; Czech, 2000; Lemmon and Ferguson, 2000; Martin, 2001; McLaughlin et al., 2002; Simonsen et al., 2001; Yin and Janmey, 2003). The importance of these lipids is highlighted by the many specialized phosphoinositide binding domains found in signaling molecules, including Pleckstrin Homology (PH), FYVE, and Phox (PX) domains (Hurley and Meyer, 2001; Lemmon, 2003; McLaughlin et al., 2002; Sato et al., 2001). Such lipid interaction domains often direct the membrane recruitment of proteins in response to the synthesis of their target phosphoinositides.

The neuronal Wiskott-Aldrich Syndrome Protein (N-WASP) is a model system for exploring the mechanism of phosphatidylinositol 4,5-bisphosphate (PIP_2) signaling. N-WASP is a key regulator of actin polymerization: it stimulates actin nucleation by the actin related protein 2/3 (Arp2/3) complex in response to upstream inputs (Higgs and Pollard, 2001; Welch and Mullins, 2002). The two best studied inputs are the small GTPase Cdc42 and PIP_2, which act in a combinatorial manner: although both are independent activators, they are far more potent when present together (Higgs and Pollard, 2000; Prehoda et al., 2000; Rohatgi et al., 1999, 2000). A recently discovered protein, Toca-1, is also thought to indirectly mediate PIP_2 control of actin polymerization, acting at a second point upstream from N-WASP (Ho et al., 2004).

Recent studies have begun to uncover the molecular mechanism of N-WASP regulation (Figure 1). The C-terminal region of N-WASP, known as VCA, serves as the core activity output domain: it can bind and stimulate the de novo actin filament nucleation activity of the Arp2/3 complex (Higgs and Pollard, 2001; Rohatgi et al., 1999; Welch and Mullins, 2002). However, in the context of the intact protein, N-WASP function is repressed through a set of autoinhibitory interactions (Kim et al., 2000; Prehoda et al., 2000; Rohatgi et al., 1999, 2000). Two N-terminal regions are required for autoinhibition, a short polybasic (B) motif and an adjacent GTPase binding domain (GBD). In the repressed state, the B motif is postulated to provide a second Arp2/3 complex binding site (Prehoda et al., 2000), whereas the GBD can bind a peptide motif within the VCA output domain (Kim et al., 2000). The composite B-GBD module is necessary and sufficient to inhibit VCA activity, presumably because this set of interactions locks the complex in an inactive state (Prehoda et al., 2000).

The input molecules PIP_2 and Cdc42 (GTP loaded) bind to the B motif and GBD, respectively, disrupting the autoinhibitory interactions and activating N-WASP. The two inputs activate synergistically, because they cooperatively compete against the autoinhibitory interactions (Prehoda et al., 2000). Although other regions of N-WASP may be important for other aspects of N-WASP function, a mini-N-WASP (mN-WASP) protein containing only the B, GBD, and VCA modules is sufficient to display cooperative coactivation by PIP_2 and Cdc42 (Figure 1B) (Prehoda et al., 2000). Moreover, mN-WASP is sufficient to drive stimulus-dependent endosome motility in *Xenopus* egg extracts (see Results).

Relatively little is known about the mechanism of the B motif. What is the affinity of the B region for PIP_2 and what is its selectivity among phosphoinositides? What is its mechanism of recognition? Finally, why does N-WASP employ this type of motif instead of larger canonical PIP_2 binding modules such as a PH domain?

Here, we show that unlike canonical PIP_2 binding modules, the basic region of N-WASP binds PIP_2 in a multivalent manner. Thus, its binding to membranes is highly sensitive to PIP_2 spatial density. Moreover, activation of N-WASP shows an even sharper dependence on PIP_2 density: N-WASP is activated in an all-or-none fashion over a very small range of increasing PIP_2 density in vitro (apparent Hill coefficient $n_H = 20$), a behavior known as ultrasensitivity (Koshland et al., 1982). The PIP_2 density dependence of activation is amplified because the B motif participates in competing autoinhibitory interactions. We demonstrate that the midpoint and the sharp-

*Correspondence: wlim@itsa.ucsf.edu
[3]Present address: Department of Chemistry, Institute of Molecular Biology, University of Oregon, Eugene, Oregon 97403.

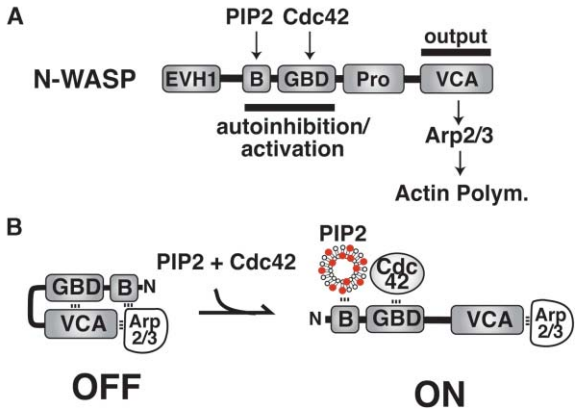

Figure 1. Mechanism of N-WASP Regulation

(A) Domain Structure of N-WASP. Arrows indicate the respective interactions of each domain with PIP_2, Cdc42, and Arp2/3 complex. The following abbreviations are used: enabled-VASP homology domain 1, EVH1; basic region, B; proline-rich sequence, Pro; verprolin homology domain, V; connecting region, C; and acidic region, A. The composite VCA domain is referred to as the output domain.

(B) Model for cooperative activation of N-WASP by PIP_2 and Cdc42. In the absence of activators, N-WASP and Arp2/3 complex are in an autoinhibited (OFF) conformation. The "OFF" state is stabilized by interaction of the GBD with the VCA domain, the basic region with the Arp2/3 complex. PIP_2 and Cdc42 act cooperatively to disrupt the autoinhibitory interactions.

ness of the PIP_2-dependent activation profile of N-WASP can be easily tuned by varying the number of lysine residues in the B motif.

Thus, the B motif appears to confer upon N-WASP an additional level of phosphoinositide signaling specificity—sensitivity to a threshold density of PIP_2. Such a mechanism may provide two functional advantages. First, it may suppress basal N-WASP activation even under the relatively high quiescent concentrations of PIP_2. Second, it may leave N-WASP sensitively poised for strong activation in response to subtle reorganization of PIP_2 in membrane domains, rather than requiring a gross change in the overall PIP_2 concentration.

Results

Binding Specificity of the N-WASP Basic Region

We measured binding of a region encompassing the B motif and the GBD (B-GBD: residues 178–274) to various phosphoinositide species with two assays (Figure 2): first, a vesicle cosedimentation assay to qualitatively assess binding (Kavran et al., 1998), and second, a fluorescence perturbation assay to quantitatively measure affinity (see Supplemental Figure S1 available online at http://www.molecule.org/cgi/content/full/17/2/181/DC1/). Binding was monitored via fluorescence change of a 7-diethylamino-3-(4'-maleimidylphenyl)-4-methylcoumarin (CPM) (Wang et al., 1999) fluorophore-labeled protein upon addition of vesicles (phosphatidyl choline [PC], phosphatidyl serine [PS], and the relevant phosphoinositide species at ratios of 70:20:10).

No detectable binding of the B-GBD fragment is observed to vesicles containing only PC/PS (80:20) or to vesicles containing PC/PS and phosphatidylinositol 4-phosphate (PI4P). Strong binding is observed to vesicles containing 10% PIP_2 (apparent $K_d \sim 1\ \mu M$). Detectable but weak binding ($\sim$10-fold lower affinity than PIP_2) is observed for vesicles containing phosphatidylinositol 3-phosphate (PI3P). Vesicles containing phosphatidylinositol 3,4-bisphosphate ($PI[3,4]P_2$) and phosphatidylinositol 3,4,5-trisphosphate (PIP_3) bind with affinities 2- to 5-fold lower than those containing PIP_2.

Thus, although the B motif binds PIP_2 with the highest affinity of the lipids tested, the specificity of this interaction is relatively low. Given that PIP_2 is estimated to be present in biological membranes at concentrations 20- to 100-fold higher than these other bis- and tris-phosphoinositide species, PIP_2 is likely to be the relevant ligand in vivo (Cantley, 2002; Czech, 2000; Fruman et al., 1999; McLaughlin et al., 2002).

Sequence Requirements for PIP_2 Binding: A Polybasic Motif

We used deletion mapping to identify smaller sequences sufficient for PIP_2 recognition (Figure 2B). Using the cosedimentation vesicle binding assay, we found that a 15 amino acid sequence from N-WASP (residues 183–197) containing ten basic residues was sufficient for binding to PIP_2-containing vesicles. This fragment displayed the lipid preferences described above for the larger 178–274 fragment (V.P., unpublished data).

To more finely map recognition requirements, we performed alanine scanning mutagenesis (Figure 2C). Surprisingly, none of the single alanine mutations had a significant impact on PIP_2 binding in the qualitative vesicle cosedimentation assay. Significant loss of PIP_2 binding was only observed when three or more basic residues were mutated to alanine.

We generated a variant of the B motif in which the amino acid sequence was reversed (identical composition) as well as polylysine sequences of 7 or 10 residues. Similar binding to PIP_2 was observed for the reverse sequence motif and the 10-lysine motif (Figure 2C), whereas no binding was observed for the 7-lysine motif. Thus, the high positive charge density of the motif, rather than any precise structure, appears to be most critical for binding. The PIP_2 binding motif from N-WASP appears to be similar to previously characterized polybasic PIP_2 binding motifs such as the basic effector domain of the myristoylated alanine-rich C kinase substrate (MARCKS) (McLaughlin et al., 2002) and distinct from larger, well-structured PIP_2 binding modules.

Affinity of the Basic Region Is Highly Dependent on PIP_2 Density

The MARCKS peptide binds multiple PIP_2 molecules and shows a cooperative binding dependence on PIP_2 density (Wang et al., 2001). We found that the binding of the N-WASP B motif is also highly dependent on PIP_2 density. We repeated our quantitative binding experiments but used vesicle preparations containing either 10% or 2% PIP_2 (Figure 3A). The observed apparent affinity is $\sim$10-fold higher when PIP_2 is present at 10% vs. 2% of total lipid ($K_d = 1.2\ \mu M$ versus $10\ \mu M$).

A direct way to examine PIP_2 density dependence is to measure binding as a function of mol% of PIP_2, a

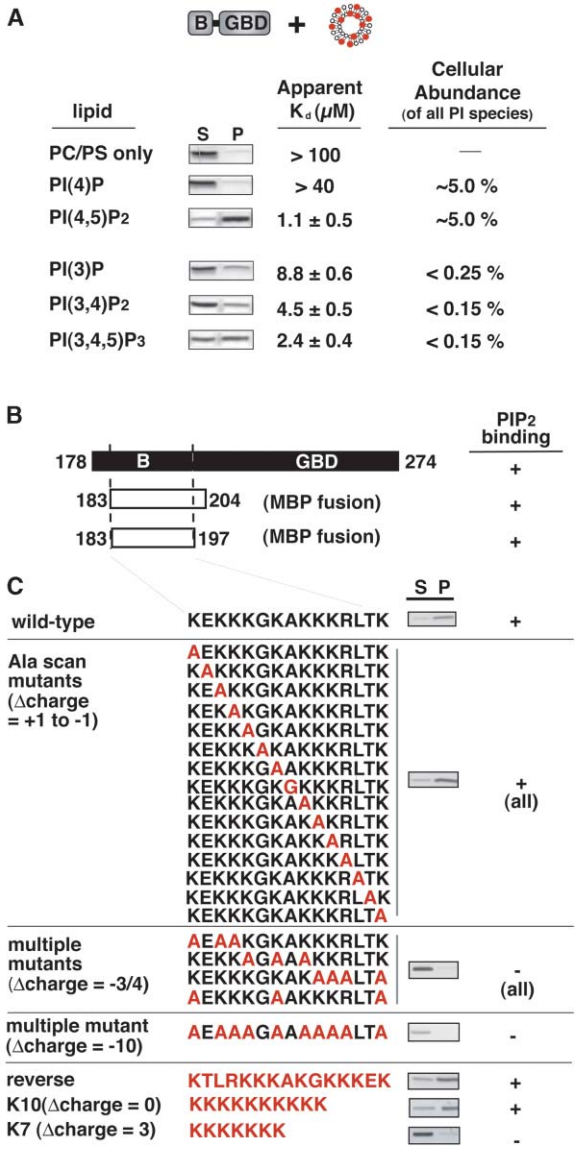

Figure 2. Specificity and Sequence Requirements of N-WASP Basic Region Binding to $PI(4,5)P_2$

(A) Indicated lipids were tested for binding to the B-GBD fragment (178–274) by two assays, a cosedimentation vesicle spindown assay, and a quantitative fluorescence binding assay (Supplemental Figure S1). S indicates supernatant (unbound), and P indicates pellet (bound). K_d (μM) was measured by fluorescence with vesicles containing PC/PS(70:20) and 10% phosphoinositide. Vesicles for spindown assay contain 5% phosphoinositide. The far right column lists the approximate cellular abundance of each species as a percentage of total phosphoinositide (Cantley, 2002).

(B) Deletion analysis of B-GBD fragment in vesicle cosedimentation binding assay shows that fragment corresponding to residues 183–197 is sufficient to selectively bind to $PI(4,5)P_2$. Deletion constructs were generated as fusions to maltose binding protein (MBP).

(C) Alanine-scanning analysis in background of B-GBD fragment (178–274). The inset shows a representative gel from the vesicle spindown assay (S, supernatant; P, pellet). None of the single residues between 183–197 are absolutely essential for PIP_2 binding. Mutation of three to four basic residues results in loss of binding. A B-GBD construct containing an N- to C-terminally reversed sequence basic region can still bind PIP_2. A Lys10 (K10) polybasic motif (fused to MBP) was able to bind PIP_2 vesicles, whereas an analogous Lys7 (K7) motif was not. Substituted residues are indicated in red.

metric for lipid surface density within a membrane (Figure 3B). This type of assay differs from our previous ones in that total lipid concentration is held constant, and only mole fraction of PIP_2 is varied. When PIP_2 binding is assayed in this way, binding of a PIP_2-specific PH domain—the domain from PLC-δ—still shows a typical hyperbolic binding isotherm indicative of noncooperative binding in a 1:1 stoichiometry. However, a fragment of N-WASP containing the B region shows a sigmoidal binding isotherm indicative of cooperative binding (Figure 3C). This curve can be fit to an apparent Hill coefficient (n_H) of ~3, similar to the binding stoichiometry observed in studies of the MARCKS basic effector domain (McLaughlin et al., 2002).

Another way to assess the effect of PIP_2 density is to alter lipid clustering. Cholesterol is thought to promote formation of lipid membrane subdomains (Sandhoff et al., 1999) and should increase the local PIP_2 density (Pike and Miller, 1998; Simons and Ikonen, 1997). Vesicles doped with 40% cholesterol bound tighter to the B region (Figure 3C). Vesicles doped with 40% cholesterol/20% sphingomyelin also showed a higher apparent affinity (V.P., unpublished data).

This multivalent mode of PIP_2 binding helps to clarify previous unexplained observations that soluble PIP_2 or IP_3 headgroup did not activate N-WASP, even when present at extremely high molar concentrations (K.E.P., unpublished data). The soluble PIP_2 derivatives probably cannot bind and activate N-WASP because they are not presented in a multivalent manner as is the case with PIP_2 in a membrane.

N-WASP Actin Polymerization Activity Shows a Threshold Dependence on PIP_2 Density

The above binding studies suggested that N-WASP activation might also be highly sensitive to the density of PIP_2. We therefore measured the in vitro activity of N-WASP (stimulation of Arp2/3-mediated actin polymerization) as a function of mol% PIP_2 in a pyrene actin polymerization assay. Assays were performed with mN-WASP (Prehoda et al., 2000), as well as a near full-length version of N-WASP lacking only the N-terminal EVH1 domain. The time required for half maximal actin polymerization ($t_{1/2}$) was used as a metric for N-WASP activity (Supplemental Figure S2).

Activation of mN-WASP showed a dependence on PIP_2 density that was even sharper than that observed for binding (Figure 3 and Supplemental Figure S3). The apparent Hill coefficient for this activation transition is n_H = ~18 (compared to n_H = ~3 for B motif binding to PIP_2). This sharp, sigmoidal activation curve is distinct from the standard hyperbolic activation curve observed when the identical mN-WASP constructs are activated by Cdc42 alone (Figure 3D, bottom). Thus, activation of mN-WASP activity by PIP_2 in vitro occurs only above a sharp density threshold. The addition of cholesterol lowers the midpoint of this activation threshold. N-WASP displays a similar cooperative activation upon addition of PIP_3 vesicles (Supplemental Figure S4). However, because of the vast excess of PIP_2 in vivo, PIP_3 is unlikely to be a relevant activator in most circumstances.

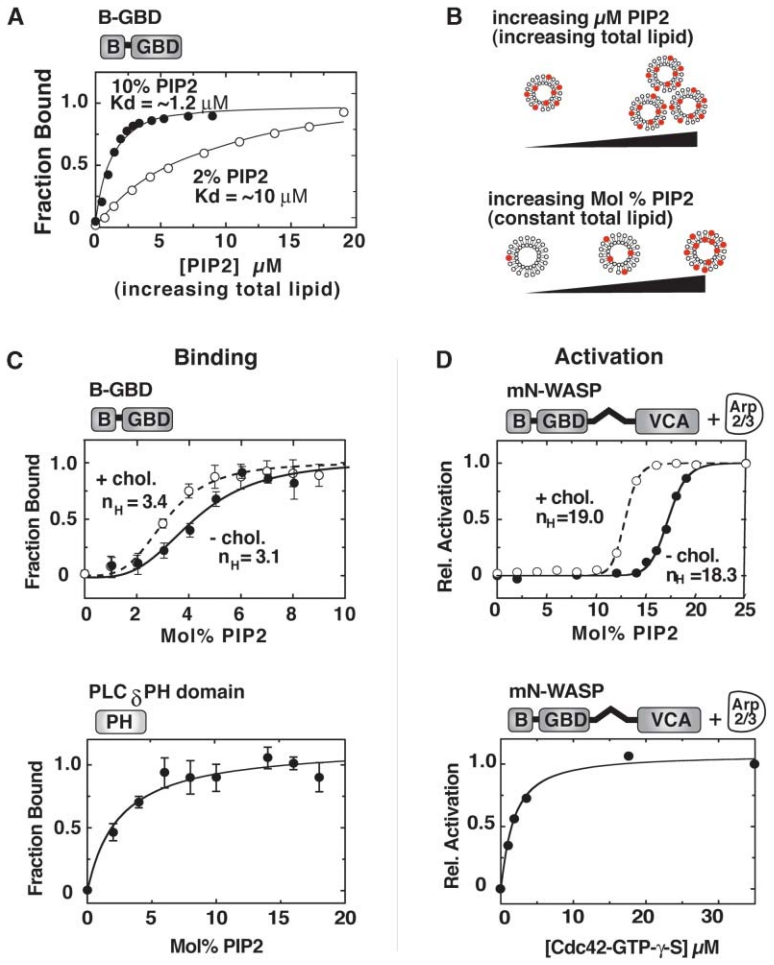

Figure 3. N-WASP Binding and Activation Is Sensitive to the Density of PIP_2 in Membranes

(A) Binding isotherms measured for B-GBD binding to PC/PS vesicles containing either 10% or 2% PIP_2. For each isotherm, % PIP_2 is held constant, but total lipid concentration is increased.

(B) Schematic of the two different vesicle binding experiments. PIP_2 concentration is increased by increasing the total concentration of lipid but keeping mol% of PIP_2 constant (top). Total lipid is kept constant, but mol% PIP_2 is increased (bottom). The latter approach detects effects of increasing PIP_2 surface density on membranes. All curves below use this latter method to perform binding or activation analysis.

(C) Comparison of PIP_2 binding isotherms for B-GBD and the PLCδ-PH domain measured with a fluorescence perturbation assay. For these assays, total lipid (PC/PS/PIP_2) is held constant at 200 μM, while PIP_2 is varied from 0–10 mol%. Assays performed in the absence of cholesterol are shown with closed circles, and assays performed with 40% cholesterol are shown with open circles. Data were fit as described in Experimental Procedures. Bars show standard deviation from three repeats. Hill coefficients (n_H) from fits are shown if they are greater than one.

(D) mN-WASP activity as a function of PIP_2 or Cdc42. Relative activity was measured by using $t_{1/2}$ values obtained in pyrene actin polymerization assays (see Experimental Procedures; raw data shown in Supplemental Figure S2). Upper curve shows activity as a function of mol% PIP_2. Closed circles are in the absence of cholesterol, and open circles are in the presence of 40% cholesterol. Lower curve shows activity as a function of Cdc42.

Autoinhibitory Interactions Amplify the Sharpness of PIP_2 Binding/Activation Threshold

The above results reveal that both B motif membrane binding and mN-WASP activation show a cooperative dependence on PIP_2 density. However, the sharpness of the mN-WASP activation profile is considerably higher than that of the B region binding profile (binding $n_H = \sim 3$; activation $n_H = \sim 20$). Moreover, the midpoint of the activation occurs at higher mol% of PIP_2 for mN-WASP activation than for B motif binding. These differences may be explained by the fact that in regulated N-WASP constructs, the B motif is occluded by competing autoinhibitory interactions, causing the apparent affinity of PIP_2 binding to be lower. Moreover, if the autoinhibitory interactions occlude multiple adjacent PIP_2 binding sites, then the cooperativity of PIP_2 binding might be higher—binding of one PIP_2 molecule to the basic motif would disrupt competing autoinhibitory interactions, thereby increasing the apparent affinity of subsequent PIP_2 molecules to adjacent sites.

A simple test of this hypothesis is to directly measure PIP_2 binding in the presence of competing autoinhibitory interactions—those of the B-GBD fragment with the VCA fragment and the Arp2/3 complex. We measured binding of mN-WASP (containing both B-GBD and VCA fragments) to PIP_2 vesicles both in the presence and absence of the Arp2/3 complex (Figure 4). The observed cooperativity of PIP_2 binding by mN-WASP was only slightly higher ($n_H = 3.8$) than that observed for binding by the B-GBD fragment alone ($n_H = 3.1$). However, if the Arp2/3 complex is also added in stoichiometric amounts, then the cooperativity of PIP_2 binding ($n_H = 17$) increases to nearly match the cooperativity of PIP_2-mediated activation ($n_H = 18$). Thus, the autoinhibitory interactions, particularly the interaction of the B motif with the Arp2/3 complex, appear to sharpen the overall PIP_2 binding and activation thresholds, consistent with the above model. These competing autoinhibitory interactions also shift the midpoint of the binding/activation threshold to higher mol% PIP_2.

Costimulation with Cdc42 Lowers PIP_2 Activation Threshold Point

We also examined how the presence of low levels of Cdc42 affects PIP_2 activation (Figure 5). We used 0.3 μM Cdc42, which by itself only yields <0.05 fractional activation of mN-WASP (see Figure 3D). The PIP_2 activation profile in the presence of this constant low amount of Cdc42 shows both a decrease in the midpoint of activation and a decrease in threshold sharpness. These observations are consistent with a model in which Cdc42 relieves the autoinhibitory interactions—Cdc42 competes against the GBD-VCA interaction and the B-Arp2/3 complex interaction (Kim et al., 2000; Prehoda

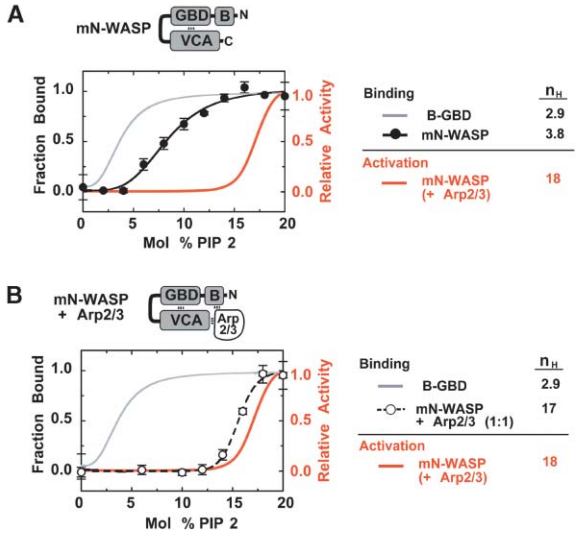

Figure 4. The Autoinhibitory Interactions in the mN-WASP-Arp2/3 Complex Amplify the Intrinsic PIP_2 Binding Cooperativity of the B Region

(A) PIP_2 binding isotherm (fluorescence binding assay) for mN-WASP. For simplicity, only the fitted binding isotherm is shown for B-GBD (data points are shown in Figure 3C).

(B) Addition of Arp2/3 increases the cooperativity of PIP_2 binding and shifts the curves to more closely resemble the cooperativity observed for mN-WASP activation (performed with Arp2/3 complex) shown in red for comparison (data points shown in Figure 3D).

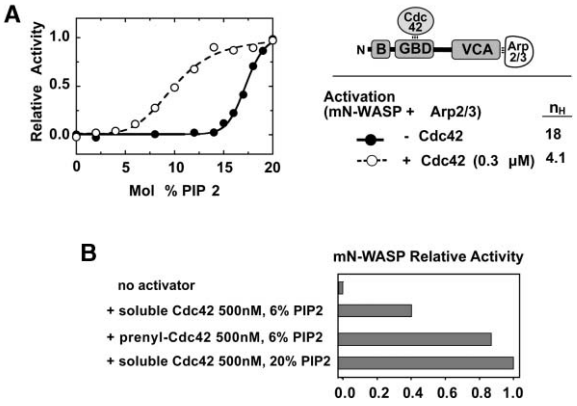

Figure 5. Soluble and Prenylated Cdc42 Can Modulate the PIP_2-Mediated Activation Profile of mN-WASP

(A) Addition of Cdc42-GTP-γ-S reduces the threshold midpoint and cooperativity for PIP_2 activation of mN-WASP. Activated Cdc42 was added at 0.3 μM.

(B) Prenylated Cdc42 is a more potent coactivator (with PIP_2) of mN-WASP than soluble Cdc42. Pyrene actin polymerization assays were performed with 2.4 μM actin, 50 nM Arp2/3, and 50 nM mN-WASP alone in the presence of 500 nM soluble Cdc42 and PC/PS vesicles doped with 6% PIP_2 or 20% PIP_2 or with PC/PS/6% PIP_2 vesicles loaded with 500 nM prenylated Cdc42. The concentration estimate for prenylated Cdc42 (active and incorporated into the vesicle) represents an upper bound estimate, because incorporation of prenyl-Cdc42 into vesicles is not necessarily quantitative. A significant fraction, however, is incorporated based on Western blotting of vesicles after centrifugation and washing.

et al., 2000) and thereby shifts the PIP_2 activation profile more toward the PIP_2 binding profile observed for the B region alone. These results indicate that small amounts of Cdc42 can reduce the PIP_2 density threshold midpoint for N-WASP activation (additional activation curves with Cdc42 and PIP_2 are shown in Supplemental Figure S5).

Endogenous Cdc42 bears a prenyl group and, thus, in vivo would be colocalized with PIP_2 at the membrane during activation. In order to better resemble physiological conditions, we loaded PIP_2-containing synthetic vesicles with prenylated-Cdc42-GTP-γ-S and tested the ability of these vesicles to activate N-WASP in actin polymerization assays. We compared these curves to results from experiments performed with soluble Cdc42 under the same conditions (Figure 5). The vesicles loaded with prenylated-Cdc42 and PIP_2 exhibited increased potency to activate N-WASP compared to similar vesicles in the presence of soluble Cdc42, indicating that colocalization of the two activators at the membrane greatly increases their cooperativity.

Changing Number of Basic Residues Can Tune N-WASP Sensitivity to PIP_2

In principle, such threshold activation behavior could be retuned by simply altering the multivalent nature of the core PIP_2 binding motif. An increase in the number of basic residues may allow it to bind more PIP_2 molecules, whereas a decrease would have the opposite effect (Wang et al., 2002).

We therefore constructed an mN-WASP variant, referred to as "14K," that contained five additional lysine residues inserted just N-terminal to the basic motif (compared to the wild-type "9K") (Figure 6). We also constructed an mN-WASP variant in which one lysine residue in the B motif was removed (K183→A), a construct referred to as "8K." Both of these mutant constructs remained repressed in the absence of activators. The 8K variant of N-WASP, however, exhibited a higher activation midpoint and decreased sensitivity compared to the wild-type, whereas the activation midpoint for the 14K variant was dramatically decreased. The 14K variant also showed an enhanced ultrasensitive response with an apparent Hill coefficient $n_H = 50$ (Figure 6).

It is possible that these additional lysine residues exert their effect not by changing the multivalency of PIP_2 binding but by weakening the overall degree of repression of the mN-WASP/Arp2/3 complex. Two observations argue against this alternative explanation. First, under basal conditions, both variant proteins were as well repressed as wild-type mN-WASP. Second, the wt and 14K mutant proteins have identical activation profiles when stimulated by Cdc42 alone (Figure 6A). These results are consistent with the model that the number of basic residues determines the multivalency of PIP_2 binding sites in N-WASP, which, in turn, can modulate the activation threshold sharpness.

Correlation between PIP_2 Sensitivity and N-WASP-Mediated Vesicle Motility

N-WASP has been shown to drive endosomal vesicle motility in *Xenopus* egg extracts (Taunton, 2001; Taunton et al., 2000). To determine if the observed threshold activation properties are relevant to the more complex process of actin-based vesicle motility, we investigated

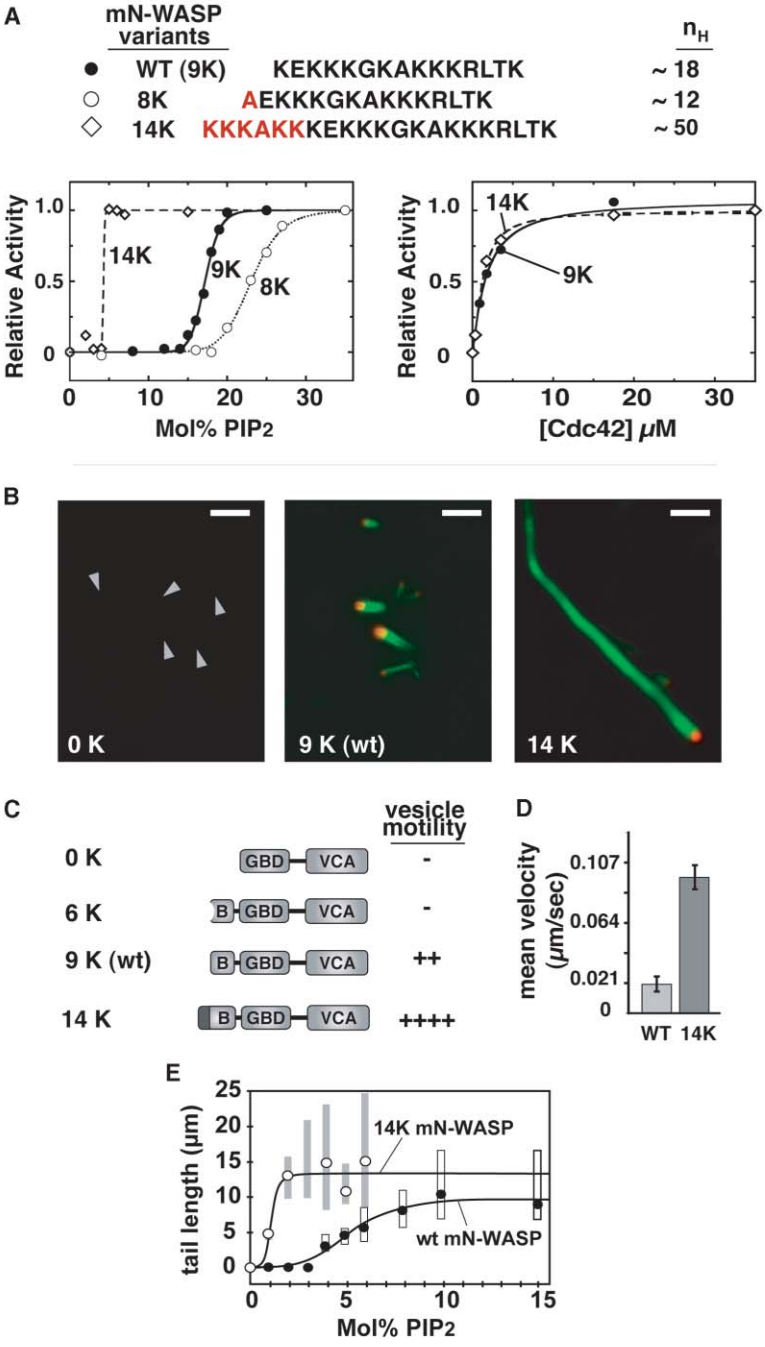

Figure 6. N-WASP Sensitivity to PIP_2 Density Can Be Tuned by Varying Charge Density in Basic Region

(A) Increasing number of basic residues in the mN-WASP basic motif lowers the activation threshold and increases threshold sharpness. Sequence changes introduced for the 8K and 14K mutants (top) compared to wt (9K). In vitro pyrene actin polymerization activation curves as a function of mol% PIP_2 were generated as described in Experimental Procedures and Figure 3 and are shown in left panel. Right panel shows activation of identical mutants by Cdc42. 14K, wt, and 8K (not shown) display virtually identical Cdc42 activation curves.

(B) Fluorescence micrographs of GBD-VCA (204-274-$[Gly\text{-}Ser]_9$-392-501), wt, and 14K mN-WASP-driven endosome motility in *Xenopus* oocyte extracts immunodepleted of native N-WASP. No motility was observed for either construct in the absence of PMA stimulation. Rhodamine-labeled N-WASP constructs are depicted in red, and FITC-labeled actin is depicted in green. 2 μm white bars are placed for reference. Arrowheads indicated nonmotile endosomes.

(C) Qualitative endosome motility (assessed by comet tail length) observed in the above assay with different mN-WASP constructs. GBD-VCA does not localize to endosomal vesicles even in the presence or absence of PMA stimulation, and no actin comets are observed.

(D) Comparison of endosome motility rates driven by wt and 14K mN-WASP. Error bars represent the standard deviation.

(E) Analysis of synthetic vesicle motility as a function of mol% PIP_2. Assays were performed with extract immunodepleted of native N-WASP but supplemented with 100 nM of wt (filled circles) or 14K mN-WASP(open circles) (no PMA stimulation). Motility was followed by assaying average actin tail length of motile vesicles under each condition. Circles represent the mean tail length, whereas bars map the tenth to ninetieth percentile range of the tail length distribution.

whether our N-WASP mutations would have similar effects on N-WASP-mediated motility. We examined the motility rates of partially purified endosomal vesicles in *Xenopus* egg extracts. In these assays, native N-WASP was immunodepleted from the extract and substituted with purified variants of mN-WASP (wt, 14K, 6K) or GBD-VCA. Motility was induced by stimulation with phorbol ester (PMA) which has been shown to induce Cdc42 activation (J.T., unpublished data). Wild-type mN-WASP is recruited to vesicles and is competent to reconstitute vesicle motility (Figures 6B and 6C). However, constructs in which the B region was deleted or constructs containing ≤6 lysine residues in the B motif did not reconstitute motility and were not even recruited to vesicles with or without PMA stimulation (Figures 6B and 6C).

Most significantly, motility was strongly enhanced by increasing the number of lysine residues. 14K mN-WASP is recruited to vesicles and yields motile vesicles with actin comet tails that are several fold longer than those generated by wt mN-WASP (Figure 6B). The average velocity of 14K-driven vesicles is ~5-fold greater than that of the wt-driven vesicles (Figure 6D). Thus, increasing mN-WASP sensitivity to PIP_2 by adding few additional basic residues also results in a corresponding increase in mN-WASP-mediated vesicle motility.

To show that the enhanced motility properties of this

mutant are due to changes in PIP_2 sensitivity, we examined the motility of synthetic vesicles in which we systematically varied the mol% PIP_2. Synthetic vesicles were added to N-WASP-depleted *Xenopus* oocyte extracts substituted with either wt or 14K mN-WASP. At sufficiently high mol% PIP_2, PMA-independent motility was observed.

Using median vesicle tail length as a metric for motility, we observed a sharp dependence of motility on PIP_2 density for both the wt and 14K proteins. Moreover, just as in the in vitro actin polymerization assays, the threshold for motility activation with the 14K protein was sharper and occurred at lower mol% PIP_2 (Figure 6E). In addition, at saturation (high PIP_2), the median length of vesicle tails was significantly longer for the 14K-driven vesicles than the wt-driven vesicles. Similar threshold behavior was observed when using the number of motile vesicles as a metric for activity, although at PIP_2 densities well above the activation threshold, the number of motile vesicles was observed to decline slightly. Overall, these data are consistent with the idea that B motif mutations directly alter motility by altering sensitivity to PIP_2 activation.

Increasing the Number of Basic Residues Results in Increased N-WASP Activity in Resting Cells

Overexpression of the enzyme phosphatidylinositol 5-phosphate kinase (PIP5K), which catalyzes the conversion of PI(4)P to PI(4,5)P_2, has been shown to induce vesicle rocketing in vivo (Benesch et al., 2002; Rozelle et al., 2000). This vesicle motility is dependent on N-WASP—it is not observed in knockout cells—and is consistent with a model in which an increase in steady-state PIP_2 level results in N-WASP activation. Rocketing vesicles show actin comet tails associated with membrane localized N-WASP.

We employed this assay to examine whether our PIP_2 hypersensitive N-WASP mutant (14K), displayed altered vesicle rocketing behavior. Cultured N-WASP$^{-/-}$ mouse fibroblast cells (Snapper et al., 2001) were transiently transfected with either wild-type or 14K N-WASP (full length). In addition, we determined the effects of cotransfecting these cells with PIP5K.

Cells transfected with PIP5K and either wt or 14K N-WASP exhibited N-WASP-associated comet tails at 66.0% and 74.6% occurrence rate, respectively (Figure 7). However, a notable difference was observed between cells transfected with either wt or 14K N-WASP in the absence of PIP5K overexpression. Whereas cells expressing exogenous wt N-WASP displayed no detectable N-WASP-associated actin comet tails (Figure 7A), 43.6% of cells expressing 14K N-WASP exhibited N-WASP-associated actin tails (Figure 7B). A movie of these rocketing vesicles in cells transfected with 14K N-WASP or wt N-WASP and GFP-actin is shown in supplemental movies (Supplemental Movie 1 and Supplemental Movie 2, respectively). These results suggest that the 14K N-WASP activation profile is altered such that a significant amount of N-WASP activation now occurs even at resting PIP_2 levels in vivo. The higher threshold activation midpoint for wt N-WASP may effectively suppress this basal activation.

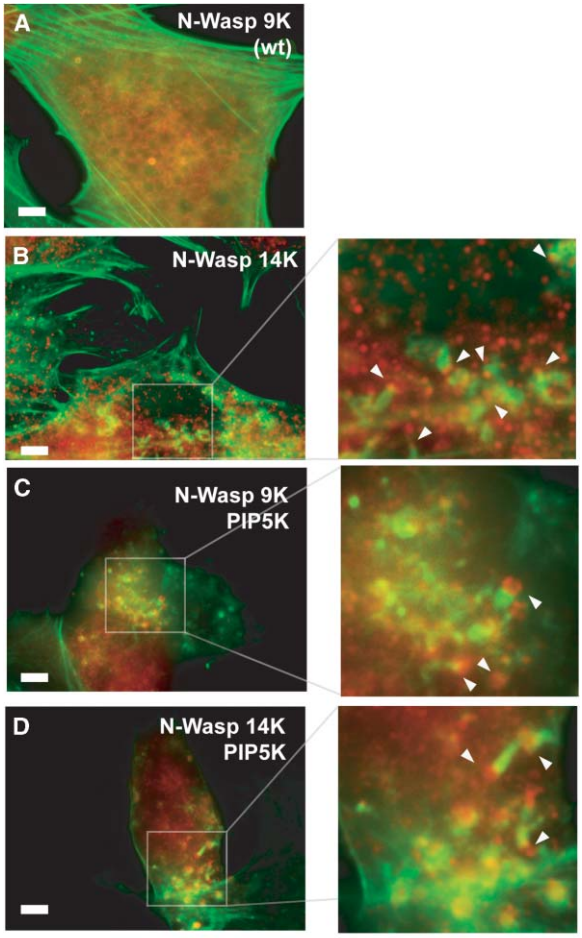

E

		% Transfected cells with tails	Motility Rate (μm/sec)
- PIP5K	N-Wasp 9K	< 5	—
	N-Wasp 14K	43.6 ± 8.1	0.12 ± 0.035
+ PIP5K	N-Wasp 9K	65.9 ± 9.0	0.19 ± 0.080
	N-Wasp 14K	74.6 ± 6.0	0.32 ± 0.093

Figure 7. N-WASP Hypersensitivity to PIP_2 In Vitro Correlates with Increased N-WASP Activity in Resting Cells

Fixed N-WASP$^{-/-}$ cells transfected with the following constructs: (A) wt N-WASP (9K); (B) 14K N-WASP; (C) wt N-WASP and PIP5K; (D) 14K N-WASP and PIP5K. Cells were stained with antibodies against N-WASP (red) and Alexa-488-phalloidin (green) to visualize actin. White arrows point to vesicles. Enlarged images are depicted on the right side of each panel. 1 μm bars are placed for reference. (E) shows the number of cells with N-WASP-associated actin comet tails. The bars represent the mean from three individual experiments in which at least 60 transfected cells were examined. Rates of motile vesicles (average of 15–20) are also given in the table. See Supplemental Movies 1 and 2.

Discussion

N-WASP Polybasic Region Confers Switch-like Sensitivity to PIP_2

These results reveal that, in vitro, the actin regulatory switch N-WASP responds to changes in PIP_2 density in a switch-like manner: the transition from the fully repressed state to the fully activated state occurs above a sharp threshold. This threshold behavior appears to

be the result of two key features of N-WASP. First, the polybasic region of N-WASP recognizes PIP_2 in a multivalent manner. Second, because the basic motif in N-WASP is also involved in regulatory autoinhibitory interactions in the repressed state, the sharpness of the PIP_2-dependent activation transition is strongly amplified. Together, these two levels of cooperativity yield a PIP_2 activation profile with an apparent Hill coefficient of ~18.

Cooperative activation has many examples in biology. For example, hemoglobin uses a homotropic allosteric mechanism to bind to O_2 in a manner sharply dependent of O_2 partial pressure (n_H = ~3) (Perutz, 1978). MAP kinase cascades in *Xenopus* oocytes appear to use several mechanisms to yield an all-or-none dose response curve (n_H = 35) (Ferrell and Machleder, 1998). Such mechanisms include successive steps of distributive multisite phosphorylation and positive feedback. Here, we have observed a different mechanism that allows N-WASP to respond in an extremely sharp manner to PIP_2 densities.

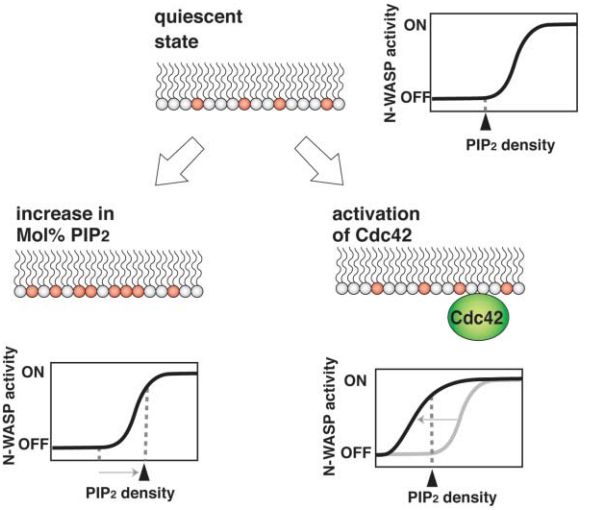

Figure 8. Steep Activation Profile of N-WASP May Balance Dampening of Activity under Quiescent Conditions with Sensitive Activation upon Subtle Input Perturbations

Under quiescent conditions (no activated Cdc42 but basal density of PIP_2), the threshold behavior of N-WASP could suppress activation. However, if quiescent densities of PIP_2 are set sufficiently close to the activation threshold, then N-WASP would be highly sensitive to activation by several possible mechanisms: small increases in PIP_2 density (<2-fold) from an increase in synthesis, decrease in decay, or membrane reorganization could lead to full activation of N-WASP (left). Alternatively, a small increase in Cdc42 could activate by shifting the activation threshold to lower mol% PIP_2. If this shift is below normal levels of PIP_2, then full activation would occur. Activation, in this case, would still be targeted specifically to the PIP_2-rich plasma membrane. Activation could also occur through a combination of increase in PIP_2 density and activated Cdc42 levels.

Noise Filtration: Possible Role of PIP_2 Activation Threshold

One function of such cooperative activation profiles may be to act as a signal filter that suppresses "leaky" activation at input doses below the threshold. This property could be particularly important for detection of PIP_2 as an activating signal. Unlike other key signaling phosphoinositides, PIP_2 is always present in the plasma membrane at relatively high concentrations, even under quiescent conditions. PIP_2 levels are estimated to be ~5–10 μM and may vary by only ±50% (0.5- to 1.5-fold) upon active signaling (Cantley, 2002; Lemmon and Ferguson, 2000; McLaughlin et al., 2002; Xu et al., 2003). In contrast, the levels of PIP_3 and $PI(3,4)P_2$ change significantly from virtually undetectable in quiescent cells to ~0.3 μM (Cantley, 2002; Carpenter et al., 1990). Given this >50-fold increase (Lemmon and Ferguson, 2000), effector proteins that bind PIP_3 by simple hyperbolic binding can still exhibit a sharp signal-dependent recruitment and activation. In contrast, if a PIP_2 effector protein binds its ligand with a simple hyperbolic activation profile, then significant "noise" levels of activity would be observed even under quiescent conditions. A hyperbolic response curve requires an ~80-fold increase in input dose (Koshland et al., 1982), a range that is not spanned by physiologically observed fluctuations in the levels of PIP_2 at the plasma membrane, to shift from 10% to 90% fractional binding or activity.

The sharp threshold observed in N-WASP activation overcomes these problems: below the threshold, noise from quiescent levels of PIP_2 could be suppressed, whereas high sensitivity to PIP_2 could be maintained at or above the threshold (Figure 8). The activation profile that we observe for mN-WASP requires only a ~1.3-fold change in mol% PIP_2 to transition from 10% to 90% activation. This small transition range is compatible with the small changes in PIP_2 density (0.5- to 1.5-fold) that are thought to occur upon signaling. It is also possible that sequestration of PIP_2 by other factors also contributes to noise filtration.

It is difficult to determine precisely how the activation properties observed from in vitro actin polymerization assays correlate with behavior in vivo, particularly the threshold setpoint in vivo. Nonetheless, our assays of vesicle motility in cytoplasmic extracts, which reflect a significantly more complex actin-based signaling process, are consistent with a sharp PIP_2 activation threshold. Synthetic vesicle motility shows a threshold dependence on mol% PIP_2, and the midpoint and sharpness of this transition is dependent on the charge density of the B region. Finally, in vivo endosome rocketing assays show that 14K N-WASP, which has an abnormally low PIP_2 activation threshold in vitro, can now be activated even by basal levels of PIP_2 (whereas wt remains inactive). This observation supports a model in which the wild-type activation threshold is normally set just above quiescent PIP_2 levels.

Multiple Modes of N-WASP Activation

The sharp activation profile of wild-type N-WASP would suppress activation under conditions of basal PIP_2 density. Nonetheless, this profile would also leave N-WASP sensitively poised for activation by several possible upstream events. First, small increases in PIP_2 density alone could trigger activation (Figure 8). Increases in PIP_2 density could occur through an increase in local PIP_2 synthesis, a decrease in its breakdown, or clustering/segregation of PIP_2 into spatial domains. This potential mode of activation may explain why overexpression

of PIP5 kinase, the enzyme that synthesizes PIP_2, results in the spontaneous formation of numerous N-WASP-mediated actin comet tails (Benesch et al., 2002; Rozelle et al., 2000). Although it remains unclear whether this mode of N-WASP activation occurs under normal physiological conditions, redistribution of PIP_2 on this scale is observed during several actin-based cytoskeletal rearrangements (Botelho et al., 2000; Marshall et al., 2001; Mayer et al., 2000).

A second possible mode of N-WASP activation is through an increase in activated Cdc42. As shown in Figure 8, even small amounts of activated Cdc42 can relieve the sharp PIP_2 response threshold. Sufficient Cdc42 could therefore yield significant activation even at quiescent PIP_2 concentrations without a significant increase in PIP_2 concentration or density. Under those circumstances, PIP_2 may function as a simple spatial rather than temporal signal, perhaps acting to specify localization to the plasma membrane. It is likely that many of the physiological events that trigger N-WASP activation may actually involve a combination of both Cdc42 activation and an increase in PIP_2 density.

This work demonstrates how a simple polybasic region has been used by nature to generate a protein switch that is activated by PIP_2 with sharp threshold properties. These properties are particularly well suited to respond to the subtle perturbations in PIP_2 that occur upon cell signaling, explaining why such a motif may be used in N-WASP instead of a folded lipid binding module such as a PH domain. It is likely that other signaling enzymes with similar input response requirements may use similar input motifs.

Experimental Procedures

Protein Expression and Purification

N-WASP fragments were amplified by polymerase chain reaction (PCR) from a rat dorsal root ganglia cDNA library and inserted into pGEX4T-1 (Pharmacia) for glutathione-S-transferase (GST) fusions, pBH4 for His6- fusions (Hillier et al., 1999), or pMAL (New England Biolabs) for maltose binding protein (MBP) fusions. Proteins were expressed in *E. coli* strain BL21 (DE3) as described (Prehoda et al., 2000).

Mutagenesis

Amino acid replacements in the basic region were introduced in a one-step polymerase chain reaction method with mutagenic 5′ oligos. The reversed B region B-GBD mutant was cloned by a two-step polymerase chain reaction method with overlapping 3′ and 5′ mutagenic oligos.

Lipid Preparation

Phosphatidyl choline (egg yolk), phosphatidyl serine (brain), PI(4)P (brain), and $PI(4,5)P_2$ (brain), were purchased from Avanti lipids (>99% pure). All other phosphoinositides (synthetic) were purchased from Echelon and Matreya (<99% pure).

Large unilamellar vesicles (LUV) were generated by mixing di(dibromostearoyl) phospatidyl choline (Avanti) and dipalmitoyl phosphatidyl-L-serine (Avanti) dissolved in chloroform in a 4:1 molar ratio. Addition of phosphoinositides was counteracted by reduction of equal moles of PC. Mixed lipids were dried over an argon stream, placed under vacuum for 30 min, and resuspended in 20 mM Hepes (pH 7.4) and 100 mM NaCl at 2.5 mM. Hydrated lipids were subjected to at least ten cycles of freeze thawing in liquid nitrogen followed by 1 min bath sonication and extrusion through a 0.1 μm filter with a lipid extruder (Avanti).

Cosendimentation Lipid Vesicle Binding Assays

Cosedimentation lipid vesicle binding assays (Kavran et al., 1998) were performed by mixing 5 μM protein and vesicles at a 20 μM final phosphoinositide concentration in 20 mM Hepes (pH 7.4), 100 mM NaCl, and 1 mM DTT (total volume = 65 μL). Reactions were incubated at 25°C for 15 min and centrifuged at 100,000 × g for 1 hr. Vesicle pellets were rinsed and resuspended in SDS-PAGE buffer of volume equal to the supernatant. Supernatant (unbound) and pellet (bound) were identified by SDS-PAGE.

Quantitative Fluorescence Vesicle Binding Assay

Purified recombinant B-GBD was labeled with a coumarin-derivative, 7-diethylamino-3-(4′-maleimidylphenyl)-4-methylcoumarin (CPM) (Molecular Probes, catalogue number D-346) at a unique Cys residue (C236). The fluorescent label was added in 10-fold molar excess in 20 mM Hepes (pH 7.5) and 100 mM NaCl and incubated O/N at 4°C, cleared by centrifugation, 2× dialysis, and gel filtration over a PD-10 column (Amersham Pharmacia).

For constant density PIP_2 titrations, lipid vesicles were titrated into a 1.5 ml solution containing 0.2 μM labeled B-GBD-CMP in 20 mM Hepes (pH 7.4), 100 mM NaCl, and 1 mM DTT with constant mixing. The sample was excited at 386 nm, and emission was detected at 457 nm (see Supplemental Figure S1).

Variable PIP_2 density binding experiments were performed in triplicate by using individual lipid vesicle 100 μl samples for each point of the titration at 0.2 μM protein and 200 μM total lipid. Data were collected on a PTI fluorometer and a Gemini XS plate reader. For mol% = 0, PC/PS vesicles were used.

Data from binding experiments were fit by nonlinear least squares methods with Profit software to the following equation:

$$I = [I_o + (I_{max} \times X^{(nH/Kd)}]/[1 + X^{(nH/Kd)}]$$

Where X is mol% PIP_2, I is the measured fluorescence intensity for that mol% PIP_2, I_o is fluorescence intensity of the unbound protein, I_{max} is the fluorescence intensity of the bound protein at saturation, n_H is the Hill coefficient, and K is the apparent binding constant. Data is plotted in figures as normalized fraction saturation Y where $Y = (I - I_o)/(I_{max} - I_o) = [X^{(nH/Kd)}]/[1 + X^{(nH/Kd)}]$. Curves were repeated three times, and standard deviations for each point are shown.

For mN-WASP binding experiments, endogenous Cys residues were mutated to Ser, and a single Cys followed by a five residue linker was introduced at the N terminus of the protein (Supplemental Figure S1). Purified protein was labeled with CPM and binding assays were carried as described for B-GBD proteins. For these assays, 0.3 μM mini-N-WASP and Arp2/3 complex were used.

To measure PLC-δ PH domain binding, we added a single Cys to the N terminus of the PLC-δ residues (1–140). The construct was expressed as a His-tagged protein, purified over a Ni-NTA resin, and labeled with CPM as described above.

Prenylated Cdc42-Vesicle Preparation

Soluble prenylated Cdc42 bound to RhoGDI was purified as described (Hoffman et al., 2000) and was incorporated into membranes by incubation with vesicles and 100 μM GTP-γ-S.

In Vitro Pyrene Actin Polymerization Assays

Experiments were performed with 2.4 μM purified rabbit skeletal muscle actin (Pardee and Spudich, 1982), 50 nM bovine Arp2/3 complex purified as described (Egile et al., 1999), and 50 nM N-WASP construct (mN-WASP, ΔEVH1 N-WASP, or VCA) in 100 μl total volume. Actin was doped with pyrene-labeled actin at 10% as described in MacLean-Fletcher and Pollard (1980) to monitor the kinetics of actin polymerization (Machesky et al., 1999). Reactions were initiated by mixing an actin mix with a premixed cocktail of Arp2/3 complex, switch, and vesicles. Final conditions were 11.5 mM imidazole (pH 7.0), 50 mM KCl, 1 mM $MgSO_4$, 1 mM EGTA, 0.2 mM ATP, 1 mM DTT, and 3 mM $MgCl_2$. Pyrene fluorescence change upon polymerization was monitored with a fluorescence plate reader (Molecular Devices).

Variable PIP_2 density activation experiments were performed at a total lipid concentration of 200 μM as in comparable binding experiments. The time required for half maximal actin polymerization

($t_{1/2}$) was used as a metric for N-WASP activity (see Supplemental Figure S2).

Endosomal Vesicle Motility Assays

Experiments were performed with high-speed *Xenopus* egg extract and purified endosomal vesicles from cultured Hela cells, prepared as previously described (Taunton et al., 2000). Extracts were depleted with anti-N-WASP antibodies, and the absence of N-WASP was confirmed by Western blot.

Purified mN-WASP proteins were labeled with rhodamine as described for CPM. Actin was labeled with Alexa(488) as previously described in Taunton et al. (2000). Samples were prepared by mixing 1 μl GLB buffer (50 mM Tris-HCl [pH 7.5], 5 mM $MgCl_2$, and 50 mM NaCl), 3.5 μl extract, 0.25 μl endosomes, 0.25 μl PMA in DMSO (4 μM final concentration), 0.5 μl mN-WASP (100 nM final concentration), and 0.25 μl labeled actin (0.25 μM final concentration). Reactions were incubated for 20 min at room temperature and examined under 600× magnification (Olympus IX70 microscope; Olympus PlanApo 60× Oil Ph3 objective lens). Data were collected 25–28 min postinduction with a Photometrics Cool Snap HQ CCD camera. For each measurement, velocity data were obtained from six vesicle tracks from 2 min movies of 13 still image frames.

Synthetic Vesicle Motility Assays

Synthetic vesicles were prepared as described above with variable mol% PIP_2. 0.25 μl of unextruded vesicles (extrusion reduces vesicle motility, because vesicle size is decreased) were mixed with a 5.5 μl of reaction mix as described above to a final lipid concentration of 100 μM. No PMA was added. All actin tails in one half of the coverslip were captured under 600× magnification, 25–30 min post reaction initiation, and images were used to determine the number of tails and tail length. For tail length measurements, data were obtained for at least 30 tails for each mol% from random images. All tails from a given image were measured (N = 30–50) to ensure against a bias in tail selection.

In Vivo Endosomal Rocketing Assays

Immortalized N-WASP$^{-/-}$ fibroblasts (Snapper et al., 2001) were cultured in DMEM at 37°C and 5% CO_2 in 24-well plates. Cells were transfected with 0.5 μg DNA with Lipofectamine 2000 by following standard protocols. Full-length rat N-WASP and mouse PIP5K-α were expressed with a pCDNA 3.1 vector. 48 hr posttransfection, cells were permeabilized with 0.1% Triton-X100, fixed with 5% paraformaldehyde, and stained with Alexa-488-phaloidin (Molecular Probes), anti-N-WASP antibody (1:200 dilution), and HRP-goat anti-rabbit secondary (1:1000 dilution). Statistical data were obtained from images (1000×) of transfected cells obtained in three individual experiments.

For live cell imaging, cells were cultured in 35 mm glass bottom microwell dishes (Mattek Corp.) transfected with 0.5 μg DNA of each construct tested in addition to 0.5 μg GFP actin (Clonetech) and, 24 hr later, were imaged with an inverted microscope in DMEM media at room temperature. Motility rates were calculated from time lapse movies (5 s intervals for 5–10 min) at 600× magnification. The motility rates from 15–22 individual actin comet tails were averaged to obtain the mean rate value.

Acknowledgments

We thank H. Bourne, E. O'Shea, D. Klopfenstein, A. Datta, R. Vale, J. Dueber, and other members of the Lim lab for useful comments on the manuscript. This work was supported by grants from the National Institutes of Health and the Packard Foundation. J.T. and C.C. are supported by the National Institutes of Health (GM66229).

Received: May 10, 2004
Revised: September 8, 2004
Accepted: November 30, 2004
Published: January 20, 2005

References

Benesch, S., Lommel, S., Steffen, A., Stradal, T.E., Scaplehorn, N., Way, M., Wehland, J., and Rottner, K. (2002). Phosphatidylinositol 4,5-biphosphate (PIP2)-induced vesicle movement depends on N-WASP and involves Nck, WIP, and Grb2. J. Biol. Chem. *277*, 37771–37776.

Botelho, R.J., Teruel, M., Dierckman, R., Anderson, R., Wells, A., York, J.D., Meyer, T., and Grinstein, S. (2000). Localized biphasic changes in phosphatidylinositol-4,5-bisphosphate at sites of phagocytosis. J. Cell Biol. *151*, 1353–1368.

Cantley, L.C. (2002). The phosphoinositide 3-kinase pathway. Science *296*, 1655–1657.

Carpenter, C.L., Duckworth, B.C., Auger, K.R., Cohen, B., Schaffhausen, B.S., and Cantley, L.C. (1990). Purification and characterization of phosphoinositide 3-kinase from rat liver. J. Biol. Chem. *265*, 19704–19711.

Czech, M.P. (2000). PIP2 and PIP3: complex roles at the cell surface. Cell *100*, 603–606.

Egile, C., Loisel, T.P., Laurent, V., Li, R., Pantaloni, D., Sansonetti, P.J., and Carlier, M.F. (1999). Activation of the CDC42 effector N-WASP by the Shigella flexneri IcsA protein promotes actin nucleation by Arp2/3 complex and bacterial actin-based motility. J. Cell Biol. *146*, 1319–1332.

Ferrell, J.E., Jr., and Machleder, E.M. (1998). The biochemical basis of an all-or-none cell fate switch in Xenopus oocytes. Science *280*, 895–898.

Fruman, D.A., Rameh, L.E., and Cantley, L.C. (1999). Phosphoinositide binding domains: embracing 3-phosphate. Cell *97*, 817–820.

Higgs, H.N., and Pollard, T.D. (2000). Activation by Cdc42 and PIP(2) of Wiskott-Aldrich syndrome protein (WASp) stimulates actin nucleation by Arp2/3 complex. J. Cell Biol. *150*, 1311–1320.

Higgs, H.N., and Pollard, T.D. (2001). Regulation of actin filament network formation through ARP2/3 complex: activation by a diverse array of proteins. Annu. Rev. Biochem. *70*, 649–676.

Hillier, B.J., Christopherson, K.S., Prehoda, K.E., Bredt, D.S., and Lim, W.A. (1999). Unexpected modes of PDZ domain scaffolding revealed by structure of nNOS-syntrophin complex. Science *284*, 812–815.

Ho, H.Y., Rohatgi, R., Lebensohn, A.M., Le, M., Li, J., Gygi, S.P., and Kirschner, M.W. (2004). Toca-1 mediates Cdc42-dependent actin nucleation by activating the N-WASP-WIP complex. Cell *118*, 203–216.

Hoffman, G.R., Nassar, N., and Cerione, R.A. (2000). Structure of the Rho family GTP-binding protein Cdc42 in complex with the multifunctional regulator RhoGDI. Cell *100*, 345–356.

Hurley, J.H., and Meyer, T. (2001). Subcellular targeting by membrane lipids. Curr. Opin. Cell Biol. *13*, 146–152.

Kavran, J.M., Klein, D.E., Lee, A., Falasca, M., Isakoff, S.J., Skolnik, E.Y., and Lemmon, M.A. (1998). Specificity and promiscuity in phosphoinositide binding by pleckstrin homology domains. J. Biol. Chem. *273*, 30497–30508.

Kim, A.S., Kakalis, L.T., Abdul-Manan, N., Liu, G.A., and Rosen, M.K. (2000). Autoinhibition and activation mechanisms of the Wiskott-Aldrich syndrome protein. Nature *404*, 151–158.

Koshland, D.E., Jr., Goldbeter, A., and Stock, J.B. (1982). Amplification and adaptation in regulatory and sensory systems. Science *217*, 220–225.

Lemmon, M.A. (2003). Phosphoinositide recognition domains. Traffic *4*, 201–213.

Lemmon, M.A., and Ferguson, K.M. (2000). Signal-dependent membrane targeting by pleckstrin homology (PH) domains. Biochem. J. *350*, 1–18.

Machesky, L.M., Mullins, R.D., Higgs, H.N., Kaiser, D.A., Blanchoin, L., May, R.C., Hall, M.E., and Pollard, T.D. (1999). Scar, a WASp-related protein, activates nucleation of actin filaments by the Arp2/3 complex. Proc. Natl. Acad. Sci. USA *96*, 3739–3744.

MacLean-Fletcher, S., and Pollard, T.D. (1980). Mechanism of action of cytochalasin B on actin. Cell *20*, 329–341.

Marshall, J.G., Booth, J.W., Stambolic, V., Mak, T., Balla, T., Schreiber, A.D., Meyer, T., and Grinstein, S. (2001). Restricted accumulation of phosphatidylinositol 3-kinase products in a plasmalemmal subdomain during Fc gamma receptor-mediated phagocytosis. J. Cell Biol. *153*, 1369–1380.

Martin, T.F. (2001). PI(4,5)P(2) regulation of surface membrane traffic. Curr. Opin. Cell Biol. *13*, 493–499.

Mayer, A., Scheglmann, D., Dove, S., Glatz, A., Wickner, W., and Haas, A. (2000). Phosphatidylinositol 4,5-bisphosphate regulates two steps of homotypic vacuole fusion. Mol. Biol. Cell *11*, 807–817.

McLaughlin, S., Wang, J., Gambhir, A., and Murray, D. (2002). PIP(2) and proteins: interactions, organization, and information flow. Annu. Rev. Biophys. Biomol. Struct. *31*, 151–175.

Pardee, J.D., and Spudich, J.A. (1982). Purification of muscle actin. Methods Cell Biol. *24*, 271–289.

Perutz, M.F. (1978). Hemoglobin structure and respiratory transport. Sci. Am. *239*, 92–125.

Pike, L.J., and Miller, J.M. (1998). Cholesterol depletion delocalizes phosphatidylinositol bisphosphate and inhibits hormone-stimulated phosphatidylinositol turnover. J. Biol. Chem. *273*, 22298–22304.

Prehoda, K.E., Scott, J.A., Mullins, R.D., and Lim, W.A. (2000). Integration of multiple signals through cooperative regulation of the N-WASP-Arp2/3 complex. Science *290*, 801–806.

Rohatgi, R., Ma, L., Miki, H., Lopez, M., Kirchhausen, T., Takenawa, T., and Kirschner, M.W. (1999). The interaction between N-WASP and the Arp2/3 complex links Cdc42-dependent signals to actin assembly. Cell *97*, 221–231.

Rohatgi, R., Ho, H.Y., and Kirschner, M.W. (2000). Mechanism of N-WASP activation by CDC42 and phosphatidylinositol 4, 5-bisphosphate. J. Cell Biol. *150*, 1299–1310.

Rozelle, A.L., Machesky, L.M., Yamamoto, M., Driessens, M.H., Insall, R.H., Roth, M.G., Luby-Phelps, K., Marriott, G., Hall, A., and Yin, H.L. (2000). Phosphatidylinositol 4,5-bisphosphate induces actin-based movement of raft-enriched vesicles through WASP-Arp2/3. Curr. Biol. *10*, 311–320.

Sandhoff, R., Brugger, B., Jeckel, D., Lehmann, W.D., and Wieland, F.T. (1999). Determination of cholesterol at the low picomole level by nano-electrospray ionization tandem mass spectrometry. J. Lipid Res. *40*, 126–132.

Sato, T.K., Overduin, M., and Emr, S.D. (2001). Location, location, location: membrane targeting directed by PX domains. Science *294*, 1881–1885.

Simons, K., and Ikonen, E. (1997). Functional rafts in cell membranes. Nature *387*, 569–572.

Simonsen, A., Wurmser, A.E., Emr, S.D., and Stenmark, H. (2001). The role of phosphoinositides in membrane transport. Curr. Opin. Cell Biol. *13*, 485–492.

Snapper, S.B., Takeshima, F., Anton, I., Liu, C.H., Thomas, S.M., Nguyen, D., Dudley, D., Fraser, H., Purich, D., Lopez-Ilasaca, M., et al. (2001). N-WASP deficiency reveals distinct pathways for cell surface projections and microbial actin-based motility. Nat. Cell Biol. *3*, 897–904.

Taunton, J. (2001). Actin filament nucleation by endosomes, lysosomes and secretory vesicles. Curr. Opin. Cell Biol. *13*, 85–91.

Taunton, J., Rowning, B.A., Coughlin, M.L., Wu, M., Moon, R.T., Mitchison, T.J., and Larabell, C.A. (2000). Actin-dependent propulsion of endosomes and lysosomes by recruitment of N-WASP. J. Cell Biol. *148*, 519–530.

Wang, J., Arbuzova, A., Hangyas-Mihalyne, G., and McLaughlin, S. (2001). The effector domain of myristoylated alanine-rich C kinase substrate binds strongly to phosphatidylinositol 4,5-bisphosphate. J. Biol. Chem. *276*, 5012–5019.

Wang, J., Gambhir, A., Hangyas-Mihalyne, G., Murray, D., Golebiewska, U., and McLaughlin, S. (2002). Lateral sequestration of phosphatidylinositol 4,5-bisphosphate by the basic effector domain of myristoylated alanine-rich C kinase substrate is due to nonspecific electrostatic interactions. J. Biol. Chem. *277*, 34401–34412.

Wang, T., Pentyala, S., Rebecchi, M.J., and Scarlata, S. (1999). Differential association of the pleckstrin homology domains of phospholipases C-beta 1, C-beta 2, and C-delta 1 with lipid bilayers and the beta gamma subunits of heterotrimeric G proteins. Biochemistry *38*, 1517–1524.

Welch, M.D., and Mullins, R.D. (2002). Cellular control of actin nucleation. Annu. Rev. Cell Dev. Biol. *18*, 247–288.

Xu, C., Watras, J., and Loew, L.M. (2003). Kinetic analysis of receptor-activated phosphoinositide turnover. J. Cell Biol. *161*, 779–791.

Yin, H.L., and Janmey, P.A. (2003). Phosphoinositide regulation of the actin cytoskeleton. Annu. Rev. Physiol. *65*, 761–789.